

Research Paper

# CIC-7 Regulates the Pattern and Early Development of Craniofacial Bone and Tooth

Yanli Zhang, Dongrui Ji, Lin Li, Shaoqing Yang, Hengwei Zhang, Xiaohong Duan<sup>✉</sup>

State Key Laboratory of Military Stomatology, National Clinical Research Center for Oral Diseases, Department of Oral Biology, Clinic of Oral Rare and Genetic Diseases, School of Stomatology, The Fourth Military Medical University, Xi'an, Shaanxi 710032, R.P. China

<sup>✉</sup> Corresponding author: Professor Xiaohong Duan, State Key Laboratory of Military Stomatology, National Clinical Research Center for Oral Diseases, Department of Oral Biology, Clinic of Oral Rare and Genetic Diseases, School of Stomatology, The Fourth Military Medical University, 145 West Changle Road, Xi'an, Shaanxi 710032, P.R. China. Tel: 86-29-84776169. Fax: 86-29-84776169. E-mail: xhduan@fmmu.edu.cn© Ivyspring International Publisher. This is an open access article distributed under the terms of the Creative Commons Attribution (CC BY-NC) license (<https://creativecommons.org/licenses/by-nc/4.0/>). See <http://ivyspring.com/terms> for full terms and conditions.

Received: 2018.09.06; Accepted: 2019.01.09; Published: 2019.02.20

## Abstract

Human *CLCN7* encodes voltage-gated chloride channel 7 (CIC-7); mutations of *CLCN7* lead to osteopetrosis which is characterized by increased bone mass and impaired osteoclast function. In our previous clinical practice, we noticed that osteopetrosis patients with *CLCN7* mutations had some special deformities in craniofacial morphology and tooth dysplasia. It is unclear whether these phenotypes are the typical features of *CLCN7* involved osteopetrosis and whether CIC-7 could regulate the development of craniofacial bone and tooth in some signaling pathways.

**Methods:** First, we collected 80 osteopetrosis cases from the literature and compared their craniofacial and dental phenotypes. Second, four osteopetrosis pedigrees with *CLCN7* mutations were recruited from our clinic for gene testing and clinical analysis of their craniofacial and dental phenotypes. Third, we used a zebrafish model with *clcn7* morpholino treatment to detect the effects of CIC-7 deficiency on the development of craniofacial and dental phenotypes. General observation, whole mount alcian blue and alizarin red staining, whole mount *in situ* hybridization, scanning electron microscope observation, lysoSensor staining, Q-PCR and western blotting were performed to observe the *in vivo* characteristics of craniofacial bone and tooth changes. Fourth, mouse marrow stromal cells were further primarily cultured to detect CIC-7 related mRNA and protein changes using siRNA, Q-PCR and western blotting.

**Results:** Over 84% of osteopetrosis patients in the literature had some typical craniofacial and tooth phenotypes, including macrocephaly, frontal bossing, and changes in shape and proportions of facial skeleton, and these unique features are more severe and frequent in autosomal recessive osteopetrosis than in autosomal dominant osteopetrosis patients. Our four pedigrees with *CLCN7* mutations confirmed the aforementioned clinical features. *clcn7* knockdown in zebrafish reproduced the craniofacial cartilage defects and various dental malformations combined the decreased levels of *col10a1*, *sp7*, *dlx2b*, *eve1*, and *cx43*. Loss of *clcn7* function resulted in lysosomal storage in the brain and jaw as well as downregulated cathepsin K (CTSK). The craniofacial phenotype severity also presented a dose-dependent relationship with the levels of CIC-7 and CTSK. CIC-7/CTSK further altered the balance of TGF- $\beta$ /BMP signaling pathway, causing elevated TGF- $\beta$ -like Smad2 signals and reduced BMP-like Smad1/5/8 signals in *clcn7* morphants. SB431542 inhibitor of TGF- $\beta$  pathway partially rescued the aforementioned craniofacial bone and tooth defects of *clcn7* morphants. The CIC-7 involved CTSK/BMP and SMAD changes were also confirmed in mouse bone marrow stromal cells.

**Conclusion:** These findings highlighted the vital role of *clcn7* in zebrafish craniofacial bone and tooth development and mineralization, revealing novel insights for the causation of osteopetrosis with *CLCN7* mutations. The mechanism chain of CIC-7/CTSK/ TGF- $\beta$ /BMP/SMAD might explain the typical craniofacial bone and tooth changes in osteopetrosis as well as pycnodysostosis patients.

Key words: osteopetrosis, CIC-7, craniofacial bone, tooth, SB431542

## Introduction

Osteopetrosis is a group of genetic disorders characterized by increased bone mass and density due to defective bone resorption [1]. Currently, the candidate genes of osteopetrosis include *IKBKG*, *CLCN7*, *OSTM1*, *TCIRG1*, *PLEKHM1*, *CAII*, *RANK*, and *RANKL* [1,2]. Human *CLCN7* encoding voltage-gated chloride channel 7 (CIC-7) is one of the key molecules involved in osteopetrosis [2-5]. In our previous study, we reported two osteopetrosis patients with *CLCN7* mutations, who had impacted teeth, enamel dysplasia, malformed teeth, altered tooth eruption and root dysplasia [6-8]. A few years later, our group and other groups showed that *Cln7* deficiency displayed dental defects in tooth eruption or root formation [7,9-11]. All of these findings provided new insights to further understand the pathological mechanisms of *CLCN7*-related osteopetrosis.

According to our previous clinical observations and some other references [12], craniofacial bone dysplasia is quite common in osteopetrosis patients. It is unclear whether these phenotypes are the typical features of *CLCN7* involved osteopetrosis and whether or how these phenotypes were caused by CIC-7 deficiency.

Some signaling molecules, including BMP, TGF- $\beta$ 1, FGF, Hedgehog, and Wnt, are involved in the regulation of craniofacial pattern [13-17]. The balance between BMP2 and TGF- $\beta$ 1 signaling pathway could be affected by cathepsin K (CTSK), which is one of the important factors for osteoclastic function and development [18]. Several studies reported that CIC-7 deficiencies in humans and mice disrupted osteoclastic function and bone resorption [19-22], and resulted in decreased lysosome luminal  $\text{Cl}^-$  concentration [23,24]. Hence, in this study, we wondered if CIC-7 could influence CTSK by changing the local luminal condition, which affects the downstream balance between BMP2 and TGF- $\beta$ 1. This remains to be a key mechanism by which CIC-7 affects craniofacial bone and tooth development.

## Methods

### Literature review of craniofacial and dental phenotypes in osteopetrosis

Related osteopetrosis references were searched to summarize the general craniofacial and dental phenotypes in osteopetrosis patients. The following keywords were used to search the references (1965 to present) from PubMed: osteopetrosis, osteomyelitis, mandible, maxilla, tooth, craniofacial, skull, and calvarium. The 58 papers in PubMed matched the searching criteria and only those references showing detailed clinical craniofacial and dental phenotypes

were included in our analysis. Finally, 80 osteopetrosis cases from 41 references were included to summarize the general characteristics of abnormal craniofacial and dental phenotypes. The genetic background for most of the cases was not mentioned (Supplementary references).

### Pedigree analysis and DNA sequencing

Five osteopetrosis patients with *CLCN7* mutations from four families were recruited in the Clinic of Oral Rare Diseases and Genetic Diseases, School of Stomatology at the Fourth Military Medical University (Xi'an, China). The patients were clinically examined and detected using different X-ray techniques including panoramic radiograph, CT, or RVG dental film as previously described [6]. The patients diagnosed with osteopetrosis demonstrated increased bone mass and frequent fractures. This study was approved by the Ethics Committee of the School of Stomatology, Fourth Military Medical University (Approval No. 2012-2-8). Informed consent was obtained from the patients and their family members. Total genomic DNA of patients and their family members was obtained from whole blood [25]. The *CLCN7* gene was amplified using polymerase chain reaction (PCR) for sequencing as described previously [26]. Sequence maps were analyzed using Sequencher software (version 5.0, Gene Codes Corporation, Ann Arbor, MI, USA). The new finding variants were identified in at least fifty healthy controls.

### Zebrafish husbandry

Embryos and adult AB strain zebrafish were raised and maintained [27]. Embryos were incubated with 0.004% 1-phenyl 2-thiourea (PTU) to avoid pigmentation. Euthanasia and handling of zebrafish in the experiments were performed according to the policies of Institutional Animal Care of the School of Stomatology, the Fourth Military Medical University.

### Morpholino injection and rescue experiments

The standard control morpholino oligonucleotide (MO) (5' - CCTCTTACCTCAGTTACAATTTATA -3') and a translation blocking MO (tbMO) by the sequence (5'-CCTGCTAAGCAGAGAACTACTGCGT -3') targeting -31 to -55 in exon 1 of zebrafish *cln7* were obtained from Gene Tools, LLC (Philomath, OR). A 1 nL of 0.25 nM *cln7* MO was injected into the embryos of zebrafish at one-cell stage using a gas-driven microinjector. The efficiency of MO was evaluated by measuring the expression of *cln7* as assessed by Q-PCR and phenotypic penetrance. The injected embryos were cultured in the embryo medium and harvested at 3 dpf (days post-fertilization) or 5 dpf for the following experiments [28].

Full-length human *CLCN7* cDNA was amplified

and subcloned into vector pCS2-EGFP. Sequencing confirmed that all the amplified sequences synthesized a complete open reading frame with EGFP sequence. The constructed vectors were digested using Not I, and the mRNAs were synthesized *in vitro* using mMESSAGE Sp6 transcription kit (Ambion, Austin, Texas, USA). MO and mRNA were co-injected into zebrafish embryos of one-cell stage. Emission fluorescence of EGFP and phenotype was observed under a fluorescence microscope (Leica M165 FC, Heidelberg, Germany).

### Qualitative transcript analysis

Total RNA was extracted from pooled 0.75 hpf (hours post-fertilization), 4 hpf, 6 hpf, 12 hpf, 1 dpf, 2 dpf, 3 dpf and 4 dpf larvae ( $n = 50$ ) using Trizol reagent (Life Technologies, Carlsbad, USA). The qualities of the isolated RNA were tested as described previously [29]. cDNA was reverse-transcribed using PrimeScript™ RT Master Mix according to the manufacturer's protocol (TaKaRa, Dalian, China). Q-PCR was performed as described [30] using specific primers listed in Table S1. The relative expression levels were calculated using the comparative threshold cycle ( $\Delta\Delta CT$ ) method.

### Whole-mount alcian blue and alizarin red staining

To detect the morphological changes of tooth and craniofacial structures, 5 dpf zebrafish embryos were collected and fixed in 4% paraformaldehyde overnight. The cartilages and mineralized tissues were stained using alcian blue and alizarin red as previously described [26]. Then, the embryos were imaged using a Leica M205 FC Stereomicroscope (Leica Microsystems Nussloch GmbH, Heidelberg, Germany). Phenotypes were quantitatively analyzed by evaluating the length of body, head, ceratohyal and palatoquadrate, the width of head and Meckel's cartilage, the distance between Meckel's cartilage and ceratohyal, and the ceratohyal angle. The amount of calcification was determined according to the intensity of red staining from the attachment point of 4V<sup>1</sup> tooth in the fifth ceratobranchial arches (cb5) of 5 dpf larvae using the NIH ImageJ software (Wayne Rasband, NIH, USA).

### In situ hybridization

Embryos were collected and fixed in fresh 4% paraformaldehyde, dehydrated in methanol and stored at -20 °C until use. *In situ* probe primers targeting Sp7 transcription factor (*sp7*) (also known as osterix),  $\alpha 1$  chain of collagen type X (*col10a1*), connexin 43 (*cx43*), distal-less homeobox 2b (*dlx2b*), and even-skipped-like1 (*eve1*) were synthesized and listed

in Table S2. All probes were amplified from cDNA derived from 2 dpf embryos and subcloned into pEASY-T3 (TransGen Biotech, Beijing, China). *In situ* probe synthesis was performed using Digoxigenin RNA Labeling Kit (SP6/T7, Roche Diagnostics, Mannheim, Germany). Whole-mount *in situ* hybridization (WISH) was performed using the standard procedure [31]. Embryos were mounted into glycerin, and imaged using Leica M205 FC Stereomicroscope (Leica Microsystems Nussloch GmbH, Heidelberg, Germany).

### Scanning electron microscope observation

Zebrafish larvae at 5 dpf were fixed in 4% paraformaldehyde overnight and stained by alcian blue and alizarin red. After that, the tooth and cb5 were isolated and incubated with 2% sodium hypochlorite for 2 min. The ultrastructure of zebrafish teeth was observed by scanning electron microscope (HITACHI S-4800, Tokyo, Japan) [27].

### Western blot

A total of 50 embryos from each group were collected at 3dpf. A 15  $\mu$ g of protein per sample was loaded into 10% SDS-PAGE gel. The following primary antibodies were used: rabbit anti-phospho-SMAD2 (Ser465/467) (138D4) monoclonal antibody (1/500, Cell Signaling, Boston, USA), rabbit anti-SMAD2 (D43B4) monoclonal antibody (1:500, Cell Signaling, Boston, USA), rabbit anti-phospho-SMAD1 (Ser463/465)/SMAD5 (Ser463/465)/SMAD9 (Ser465/467) (D5B10) monoclonal antibody (1:1000, Cell Signaling, Boston, USA), rabbit anti-SMAD1/5/9 (ab66737) polyclonal antibody (1:500, Abcam, Cambridge, England), rabbit anti-CTSK polyclonal antibody (1:500, Proteintech, Chicago, USA), and mouse anti-GAPDH monoclonal antibody (1:1000, Sigma, St. Louis, Missouri, USA). Secondary antibodies included horseradish peroxidase (HRP)-conjugated goat anti-mouse and goat anti-rabbit secondary antibodies (Cowbio, Beijing, China). Chemiluminescence signals were detected by ChemiDoc MP (Bio RAD, California, USA). Signals were quantified with ImageJ (Wayne Rasband, NIH, USA).

### LysoSensor staining

Live 3 dpf embryos were incubated with 1  $\mu$ M LysoGreen (KeyGen Biotech, Nanjing, China) in embryo media for 30 min at 28.5 °C in dark. Embryos were then rinsed three times using fresh embryo media, and observed by using fluorescence microscopy (Leica M165 FC, Heidelberg, Germany).

### Primary culture of mouse bone marrow stromal cells (BMSCs) and *Cln7* siRNA transfection

Six-week-old male Balb/c mice were sacrificed by

cervical dislocation. BMSCs were flushed from the femur and tibia, and then were cultured with  $\alpha$ -MEM (Gibco, Grand Island, NY, USA) medium containing 20% FBS (Hyclone, Logan, Utah, USA). The protocol has been described in our previous studies [32].

The small interfering RNA (siRNA) duplexes targeting the mouse *Cln7* gene was designed and synthesized by GenePharma (Shanghai, China) according to GenBank™ (NM\_011930.3). The sequences of *Cln7* siRNA were as follows: sense, 5'-GAGGAGGA AAGACGAAUCATT-3'; antisense, 5'-UGAUUCGU CUUCCUCCUCTT-3'. The control siRNA was used as the following: sense, 5'-UUCUCCGAACGUGUCA CGUTT-3'; antisense, 5'-ACGUGACACGUUCGGAG AATT-3'.

The 2nd passage BMSCs that reached up to 80% confluence were transfected with *Cln7* siRNA or control siRNA using lipofectin 2000 (Invitrogen, Carlsbad, USA). After 48 h, the cells were collected for Q-PCR and western blot analysis. The primers were listed in Table S1.

## Drug Treatments

SB431542 (Selleck, Houston, USA), an effective inhibitor of the canonical TGF- $\beta$  pathway, was dissolved at a concentration of 10  $\mu$ M in DMSO. Control MO or *cln7* MO was injected into zebrafish embryos at one-cell stage. Then, 10  $\mu$ M SB431542 was added at 14- to 15-somites stage and equal amount of DMSO was used as control. The culture medium was changed every 48 h and 5 dpf embryos were used for whole-mount alcian blue and alizarin red staining.

## Results

### Clinical craniofacial and dental characteristics of osteopetrosis patients

Among the 80 reviewed osteopetrosis cases, there were 51 autosomal recessive osteopetrosis (ARO) and 29 autosomal dominant osteopetrosis (ADO) patients, respectively. The typical craniofacial features of these osteopetrosis patients included macrocephaly, trapezoidal shape of head, frontal bossing, changes in the shape and proportions of facial skeletons and abnormal lateral and superior orbital walls. X-ray of calvarium showed thickened and three-layer calvarium, or hair-on-end appearance. Absence or poor pneumatization of sinuses, nasal obstruction and hypertelorism were commonly observed in the middle of the face and sinuses. Mandibular malformation was characterized by mandibular hypoplasia, widened and deepened mandible with increased gonial angle and short mandibular body. The abnormalities associated with tooth included malformed roots and crowns, missing

teeth, poorly calcified teeth, abnormal pulp spaces, absence of tooth buds, caries, and enamel dysplasia. All of the above changes were more frequently observed in ARO than in ADO (Table 1). Other craniofacial abnormalities included osteomyelitis, necrotic bone and fistulae. The ratios of osteomyelitis in ARO and ADO were 47% and 34%, respectively.

**Table 1.** Summary of craniofacial and tooth abnormalities in osteopetrosis patients from literature review.

Abnormalities	ARO (cases, %)	ADO (cases, %)	Total (cases, %)
Tooth	45/51 (88%)	22/29 (76%)	67/80 (84%)
Mandible	33/51 (65%)	9/29 (31%)	42/80 (53%)
Middle of face and sinuses	28/51 (55%)	8/29 (28%)	36/80 (45%)
Osteomyelitis	24/51 (47%)	10/29 (34%)	34/80 (43%)
Fistulae	13/51 (26%)	6/29 (21%)	19/80 (24%)
Calvarium	32/51 (63%)	9/29 (31%)	41/80 (51%)
Frontal bossing	28/51 (55%)	6/29 (21%)	34/80 (43%)
Shape and proportion of the facial skeleton	38/51 (75%)	13/29 (45%)	51/80 (64%)
Hearing	18/51 (35%)	5/29 (17%)	23/80 (29%)

ARO: autosomal recessive osteopetrosis, ADO: autosomal dominant osteopetrosis.

### Craniofacial and dental characteristics of osteopetrosis patients with *CLCN7* mutations

Family A presented an autosomal dominant pattern of inheritance (Figure 1A). The proband II<sub>1</sub> was diagnosed with osteopetrosis at the age of four. His major clinical symptoms included multiple fractures, anemia and interventricular septal defect, malocclusion (Figure 1D), mandibular osteomyelitis, facial bone dysplasia, and increased bone mineral density (Figure 1B-C). The proband carried c.746C>T (p. Pro477Leu) mutation in *CLCN7* gene. His brother (II<sub>3</sub>) showed increased bone mineral density of the spine without other obvious symptoms and craniofacial malformations (Figure 1E<sub>1</sub>, E<sub>2</sub>). His mother (I<sub>2</sub>) and daughter (III<sub>1</sub>) carried the same mutation, but showed no obvious clinical symptoms.

The proband (II<sub>1</sub>) in family B was 29 years old. Her radiographs revealed a general increase of bone density in the jaws, clavicle and ribs. Her major symptoms included delayed growth rate, short stature, multiple bone fractures and severe anemia. The main craniofacial features included recurrent osteomyelitis in the facial region, malocclusion, maxillofacial and mandibular dysplasia, macrocephaly and frontal bossing (Figure 1F-K). The proband presented compound heterozygous mutations in *CLCN7* gene (c.856C>T, p. Arg286Trp; c.1430T>C, p. Leu 477 Pro) and the variant c.1430T>C in exon 16 was inherited from her mother (Figure 1A). Her mother reported no obvious clinical symptoms. Detailed information about family C and family D was reported previously [6], and the two probands have typical craniofacial and tooth features including osteo-

myelitis and unerupted teeth with root dysplasia.

To sum up, the craniofacial and dental features in the four pedigrees with *CLCN7* mutations, three cases (II<sub>1</sub> in family A, family B and family C, respectively) presented typical craniofacial features of osteopetrosis such as macrocephaly, frontal bossing, and changes in shape and proportions of facial skeleton. The cases belonged to intermediate

autosomal osteopetrosis (IRO) or severe ADO type II (ADO II), and their craniofacial features matched the general osteopetrosis analysis results. Meanwhile, clinical variations, even in a pedigree with the same *CLCN7* mutation, were observed, which were consistent with the previous report [33]. More details of craniofacial and dental features in the four pedigrees were presented in **Table 2**.

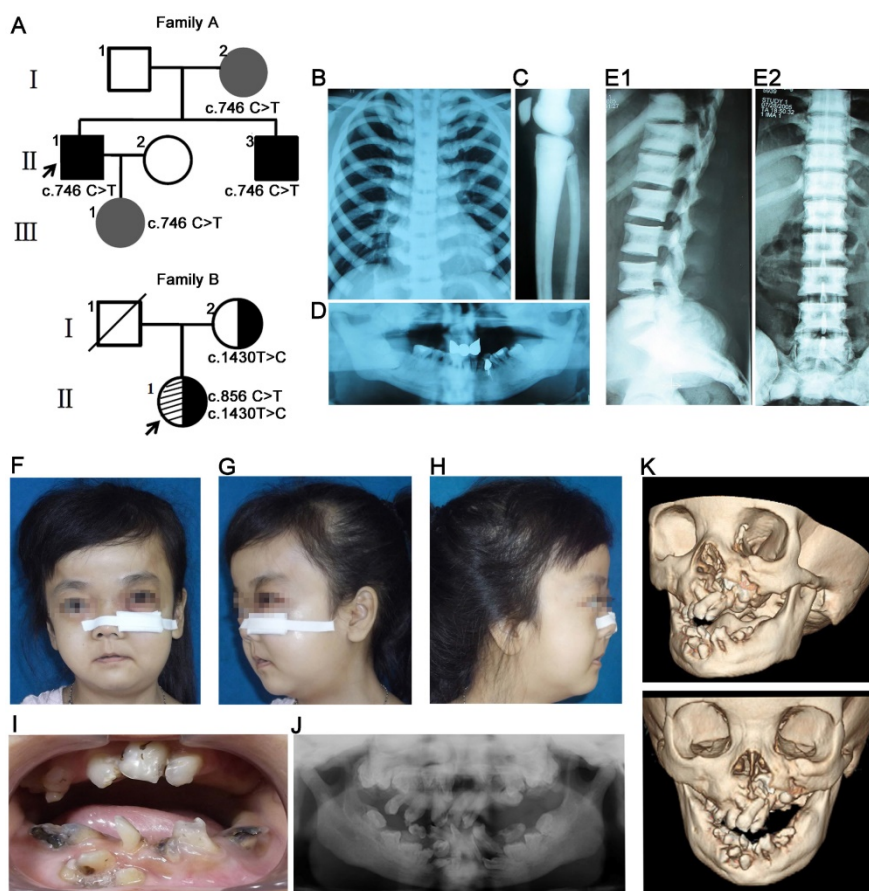


**Figure 1. Pedigree and clinical examinations.** (A) Pedigree maps. Family A presented an autosomal dominant pattern of inheritance with c.746C>T mutation in *CLCN7* gene. Black and grey represented severe phenotypes and no complaint of symptoms, respectively. The proband (II<sub>1</sub>) in family B carried compound heterozygous mutations in *CLCN7* gene (c.856C>T; c.1430T>C) and the variant c.1430T>C in exon 16 was inherited from her mother. (B-D) Radiographic images of II<sub>1</sub> in family A. Increased bone density in chest (B) and long bones (C). Malformation of craniofacial bones and tooth abnormalities in orthopantomography of II<sub>1</sub> (D). (E1-E2) Radiographic images of II<sub>3</sub> in family A. Sandwich vertebral changes. (F-K) Clinical images of individual II<sub>1</sub> in family B. (F-H) Typical craniofacial deformities including macrocephaly, frontal bossing, and changes in shape and proportions of facial skeleton. Osteomyelitis and fistulae in the left facial bones. (I-J) Intraoral photography and orthopantomography showed malocclusion and tooth malformation. (K) Hypoplasia of facial skeletons from CT images.

**Table 2.** Information of individuals with *CLCN7* mutations.

Family No.	DNA Nucleotide Change (NM_001287.5)	Predicted Protein Change (NP_001278.1)	Genotype	Subtype	Radiographic changes	Anemia	Craniofacial Phenotypes	Dental Phenotypes	Age at diagnosis
A	I <sub>2</sub> c.746C>T	p.Pro249>Leu	heterozygous	asymptomatic	mild	absent	absent	absent	N/A
	II <sub>1</sub> c.746C>T	p.Pro249>Leu	heterozygous	ADO II	serve	moderate	moderate	moderate	4 years old
	II <sub>3</sub> c.746C>T	p.Pro249>Leu	heterozygous	ADO II	serve	absent	mild	mild	7 years old
	III <sub>1</sub> c.746C>T	p.Pro249>Leu	heterozygous	asymptomatic*	mild	absent	absent	absent	N/A
B	I <sub>2</sub> c.1430T>C	p.Leu477Pro	heterozygous	asymptomatic	N/A	absent	absent	N/A	N/A
	II <sub>1</sub> c.856C>T; c.1430T>C	p.Arg286Trp; p.Leu477Pro	compound heterozygous	IRO	severe	severe	severe	severe	3-4 years old
C	I <sub>2</sub> c.1409C>T	p.Pro470Leu	heterozygous	asymptomatic	N/A	absent	absent	N/A	N/A
	II <sub>1</sub> c.1409C>T	p.Pro470Leu	homozygous	IRO	severe	severe	severe	severe	6-7 years old
D	II <sub>1</sub> c.856C>T	p.Arg286Trp	heterozygous	ADO II	moderate	absent	moderate	moderate	6 years old

N/A: not available; \* polydactyly; IRO: intermediate autosomal osteopetrosis; ADO II: autosomal dominant osteopetrosis, type II.

## Spatial and temporal expression of *clcn7* in early zebrafish development

As shown in **Figure 2A**, the maternal mRNA signals of *clcn7* were detected during the cleavage stage of the embryos (4 cell, 8 cell), and then ubiquitously expressed during the blastula period (4 hpf). Expression of *clcn7* was confined to the enveloping layer (EVL) surrounding the embryo during the gastrula and bud stages (7 hpf, 10 hpf). The positive expression location of *clcn7* was present in the head including brain, eye and jaw from 1 dpf to 4 dpf. An intensive expression was also found in the ceratobranchial arches at 4 dpf. The consistent transcript level of *clcn7* was confirmed by Q-PCR (**Figure 2B**). This expression pattern suggested that *clcn7* might be involved in the development of brain, eye or craniofacial bone.

## CLC-7 deficiency causes zebrafish craniofacial defects

According to our clinical data analysis, ARO and ADO II cases with *CLCN7* mutations showed specific malformations of craniofacial bones and mandibles. Consistently, knockdown of *clcn7* by morpholino in zebrafish embryos resulted in shorter body, smaller head and craniofacial abnormalities when compared with control, MO-injected embryos (**Figure 3A-B**). To evaluate the efficiency of MO, *CLCN7* mRNA containing *clcn7* MO target sequence were co-injected

into embryos, and the results showed rescuing of craniofacial phenotypes (**Figure 3A-B**). These data indicated that *clcn7* was required for patterning of zebrafish craniofacial skeleton.

There were a series of craniofacial cartilage defects in *clcn7* morphants, including altered ceratohyal (Ch) angle (**Figure 3A, C-D**), increased distance from Meckel's cartilage (M) to Ch and shorter length of Ch and palatoquadrate (Pq) (**Figure 3F**), which may contribute to shorter head. In contrast to control morphants, *clcn7* morphants displayed the defects or even loss of ceratobranchial arches (**Figure 3A**), and enlarged or inversed Ch angle (**Figure 3A, D**). Interestingly, the position of otolith was also changed in *clcn7* morphants with comparable calcification degree (**Figure 3A, E**).

*clcn7* morphants demonstrated hypocalcification of most of the bones with weak red alizarin red staining (**Figure 3A**). WISH and Q-PCR analysis confirmed significant decrease in the expression levels of *sp7* and *col10a1* (**Figure 3G-H**) in *clcn7* morphants. Thus, these evidences confirmed that *clcn7* was crucial for craniofacial development and mineralization in zebrafish, explaining the craniofacial abnormalities in human osteopetrosis involved *CLCN7* mutations. There was a wide variety of the aforementioned craniofacial abnormalities in *clcn7* MO group, which mimicked the variable phenotypic changes in osteopetrosis cases with *CLCN7* mutations.

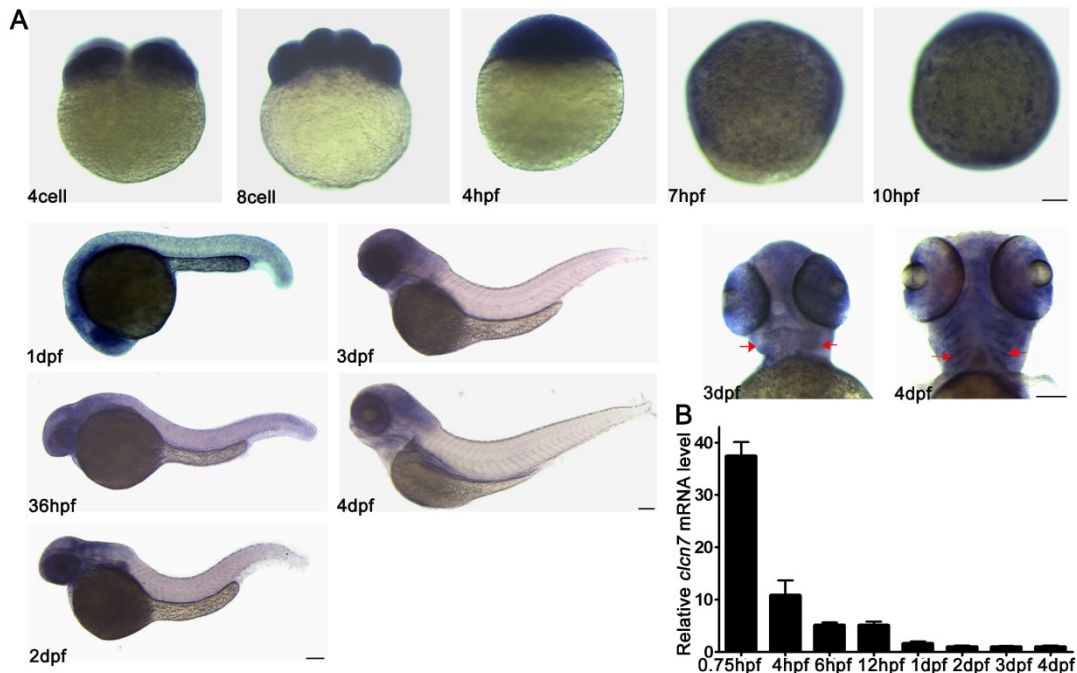


**Figure 2. Spatial and temporal expression patterns of *clcn7* during zebrafish early development. (A)** WISH results. *clcn7* was detected during cleavage stage (4 cell, 8 cell) in whole cells at blastula stage (4 hpf), especially in the enveloping layer at gastrula and bud stages (7 hpf, 10 hpf) in the head of embryos from 1 dpf to 4 dpf. Strong signaling appeared in pharyngeal arches from the ventral portion (3 dpf, 4 dpf). **(B)** Q-PCR results of *clcn7*. The red arrow indicates pharyngeal arches. dpf: days post-fertilization. hpf: hours post-fertilization. Error bars represent standard deviation. Each experiment was repeated at least three times. Scale bars: 100  $\mu$ m.

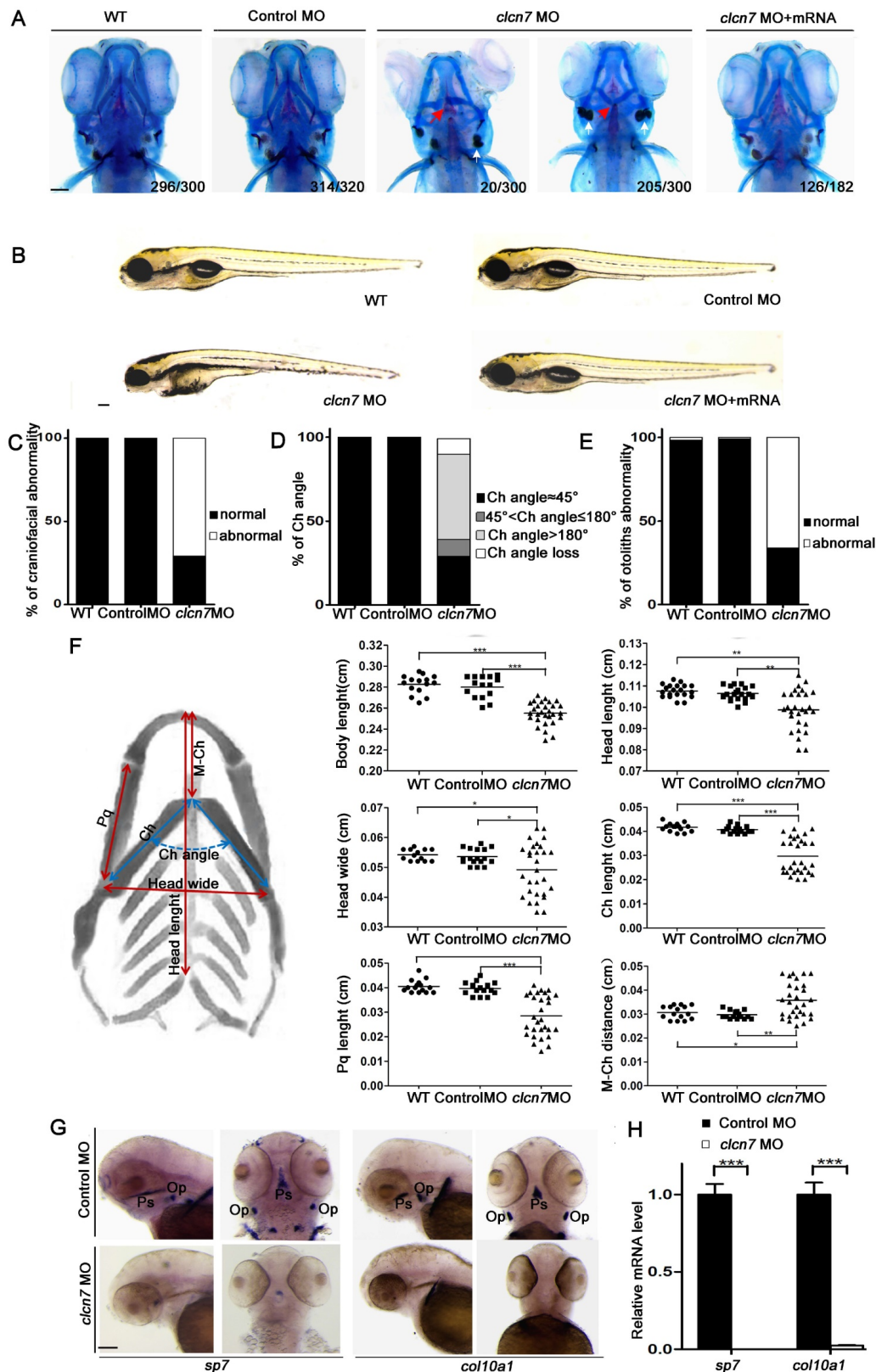


**Figure 3. Craniofacial bone and cartilage abnormalities in *clcn7* morphants.** (A) Craniofacial phenotype comparison between control and *clcn7* morphants. Cranial cartilages (blue) and mineralized bones (red) were stained with alcian blue and alizarin red in control and *clcn7* morphants at 5 dpf, respectively. (A-C) Compared to WT and Control embryos, *clcn7* morphants showed more malformed craniofacial skeletons, and *clcn7* mRNA rescued the abnormalities in craniofacial region. (D, E) Abnormal ceratohyal (Ch) angle and altered location of otolith in *clcn7* morphants. (F) Quantitative analysis of a series of changes of phenotypic indexes. *clcn7* morphants showed obvious changes in the pattern of craniofacial structure. (G) WISH analysis showed the abolished expression of *sp7* and *col10a1* in cranial skeleton, most notably in the parasphenoid (Ps) and opercle (Op) bones in *clcn7* morphants at 3 dpf. (H) Q-PCR analysis confirmed the reduced level of *sp7* and *col10a1*. For A-E, WT n=300, Control MO n=320, *clcn7* MO n=300, *clcn7* MO + mRNA n=182. For H: Control MO n=50, *clcn7* MO n=50. The red arrow indicates abnormal Ch angle, and the white arrow points to abnormal otolith. Ch: ceratohyal. M: Meckel's. Op: opercle. Pq: palatoquadrate. Ps: parasphenoid. WT: wide type. Error bar represents the SD. The experiment was repeated at least thrice with the same conditions. \*  $p < 0.05$ , \*\*  $p < 0.01$ , \*\*\*  $p < 0.001$ . Scale bars: 100  $\mu$ m.

## Loss of *clcn7* function leads to zebrafish tooth defects

According to the aforementioned clinical analysis, osteopetrosis patients with/without *CLCN7* mutations showed a higher rate of defective teeth. Consistent with these findings, we also observed significant changes in tooth shape and number of *clcn7* morphants. Histological staining revealed that teeth 3V<sup>1</sup>, 4V<sup>1</sup> and 5V<sup>1</sup> with regular morphology were conspicuously found in the control morphants at 5dpf (**Figure 4A**). In contrast, only 70% *clcn7* morphants had 4V<sup>1</sup> tooth and 30% of them had 3V<sup>1</sup> and 5V<sup>1</sup> tooth (**Figure 4A, C**). The configuration of teeth was also malformed and exhibited decreased calcium deposition in *clcn7* morphants (**Figure 4A-B**). SEM observation demonstrated that the control tooth 4V<sup>1</sup> presented smooth and coherent surface, whereas rough and porous surface was visible in the teeth of *clcn7* morphants (**Figure 4D**).

To better understand the involvement of CIC-7 mechanisms of tooth defects, several markers of tooth development were assessed including *dlx2b*, a tooth epithelium and mesenchymal marker [34], *cx43*,

expressed in odontoblasts and ameloblasts [34], *eve1*, expressed in ameloblasts of 4V<sup>1</sup> [35], and *sp7*, a marker for tooth and osteoblast differentiation [36]. WISH analysis showed that all *dlx2b*, *cx43*, *eve1* and *sp7* genes were prominently abolished in *clcn7* morphants (**Figure 5A** and **Figure 3G**), and Q-PCR confirmed the downregulation of *dlx2b*, *cx43*, *eve1* and *sp7* with *clcn7* deficiency (**Figure 5B** and **Figure 3H**). These results illustrate that knockdown of *clcn7* affected tooth development and calcification including enameloid changes in zebrafish.

## Lysosomal abnormalities and reduced CTSK expression in *clcn7* deficient zebrafish

CIC-7 is localized in late endosomes and lysosomes, and its deficiencies led to defective lysosome in mammals [23]. There was a pronounced increase of LysoTracker intensity in the head of *clcn7* morphants, especially in the brain and jaw, whereas no noticeable signals were detected in the control morphants (**Figure 6A**). This implied that *clcn7* deficiency also led to impaired lysosomal function in zebrafish.

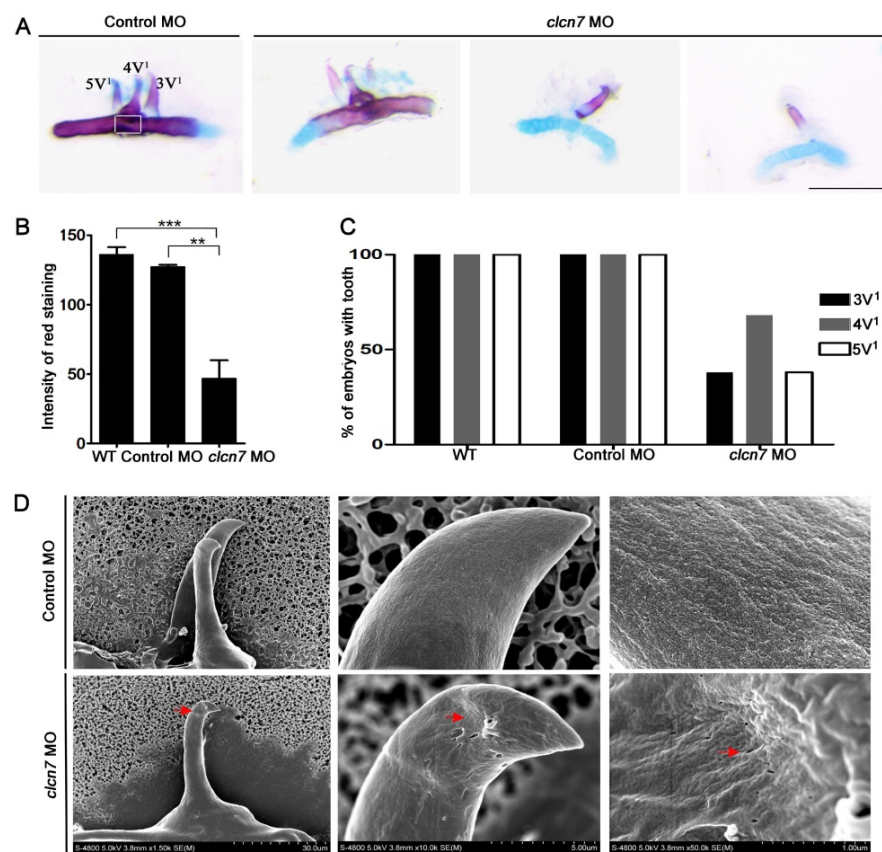


**Figure 4. Defective tooth phenotypes in *clcn7*-deficient zebrafish.** (A) Alcian blue and alizarin red staining results of 5<sup>th</sup> ceratobranchial arch and teeth in control and *clcn7* morphants at 5dpf. The malformed teeth were fewer with weak red staining *clcn7* morphants. (B) Quantitative comparison of the extent of calcification among WT embryos, control and *clcn7* morphants. (C) Comparison of embryonic tooth number. WT and control embryos had 3V<sup>1</sup>, 4V<sup>1</sup> and 5V<sup>1</sup> teeth, while *clcn7* morphants showed 3V<sup>1</sup>, 4V<sup>1</sup> and 5V<sup>1</sup> fewer teeth. (D) Ultrastructure of tooth 4V<sup>1</sup> in control and *clcn7* morphants. *clcn7* morphants had malformed tooth and enameloid dysplasia. Red arrows point to the pits on the enameloid surface. For A, B, D: WT n=50, Control MO n=50, *clcn7* MO n=50. The white square in the first image of figure A is the region for measuring calcified content in panel B. Error bar represents the SD. The experiment was repeated thrice with the same conditions. The data in image C was one of the representative experimental results. WT n=300, Control MO n=320, *clcn7* MO n=300. \* p<0.01, \*\*\* p<0.001. Scale bars: 100  $\mu$ m.

It has been reported that perturbation of lysosomal function leads to alterations in the activity of cathepsin proteases such as CTSK. Not surprisingly, we detected a remarkable decrease of CTSK in *clcn7* morphants (Figure 6B), which was consistent with the previous report regarding the reduced expression of CTSK mRNA in ADO II patient [37].

As varied craniofacial changes of *clcn7* morphants were found, we wondered whether the *clcn7* expression level showed a dose-dependent effect on the phenotypes of craniofacial bones. *clcn7* morphants were divided into severe and mild groups according to the major changes in Ch angle and severe group had the reversal Ch angle (Ch angle >180°). The expression level of *clcn7* was lower in the severe group than in the mild group. The *ctsk* mRNA level was parallelly down-regulated in the *clcn7* morphants with severe craniofacial changes (Figure 6C). These findings manifested new insights into the role of CTSK in CLCN7-related osteopetrosis.

### CIC-7 deficiency disrupted the balance between BMP signaling and TGF- $\beta$ signaling

The transcript levels of *bmp2b*, *bmpr1ba*, *bmpr1bb*, *bmpr2a*, and *bmpr2b* (Figure 6D) as well as BMP downstream signaling phosphorylated SMAD1/5/8 (pSMAD1/5/8) showed significant reduction in *clcn7*

morphants (Figure 6F). TGF- $\beta$ -propagated Smad2/3 signals usually balanced the changes of BMP-regulated Smad1/5/8 signals in matured chondrocytes [38]. Unsurprisingly, the levels of phosphorylated SMAD2 (pSMAD2) and *tgfbr2a* were prominently higher in *clcn7* morphants compared to controls (Figure 6E, G). These data demonstrated that knock-down of *clcn7* led to unbalance between TGF- $\beta$  and BMP signaling, which, therefore, changed the pattern and development of craniofacial bone and tooth in zebrafish.

### CIC-7 deficiency caused similar CTSK/BMP changes in mouse BMSCs

After *Clcn7* siRNA transfection, the expression of *Clcn7* in BMSCs was downregulated. Subsequently, the mRNA expression levels of *Ctsk* were decreased in BMSCs, and so did the expression levels of *Bmp2*, *Bmpr1a*, *Bmpr1b* and *Smad1* (Figure 6I). The protein level of pSMAD1/5/8 was reduced and that of pSMAD2 was increased in *Clcn7* deficiency BMSCs, respectively (Figure 6J, K).

### SB431542 inhibitor of TGF- $\beta$ pathway rescued the craniofacial defects of *clcn7* morphants

Imbalance in TGF- $\beta$ /BMP signaling contributes to craniofacial phenotypes of *clcn7* morphants, while the disruption of this imbalance might rescue some other phenotypes. As the level of TGF- $\beta$ -propagated Smad2/3 signals was relatively increased, SB431542, a selective small molecule inhibitor of the activin receptor-like kinase (ALK)-4, ALK-5, and ALK-7, has been shown to selectively block TGF- $\beta$ 1 signaling by preventing phosphorylation of SMAD2 without affecting BMP signaling [39-41]. To avoid perturbations in the early developmental roles of TGF- $\beta$  family signaling, embryos were treated with 10  $\mu$ M SB431542 during 14- to 15-somite stages. Compared to the controls (Figure 7A), most *clcn7* MO embryos exhibited enlarged or inversed Ch angle (Figure 7B). SB431542-treated *clcn7* morphants exhibited partial restoration of Ch angle (Figure 7D). Quantitation of changes in phenotypic severity revealed a significant shift in the number of mutants from severe to mild phenotypes. Under DMSO treatment, the *clcn7* deficient embryos with enlarged Ch angle and inversed Ch angle were 16.67% and 52.22%, respectively (Figure 7I). Under SB431542 treatment, the *clcn7* deficient embryos with enlarged Ch angle and inversed Ch angle were switched to 66.67%

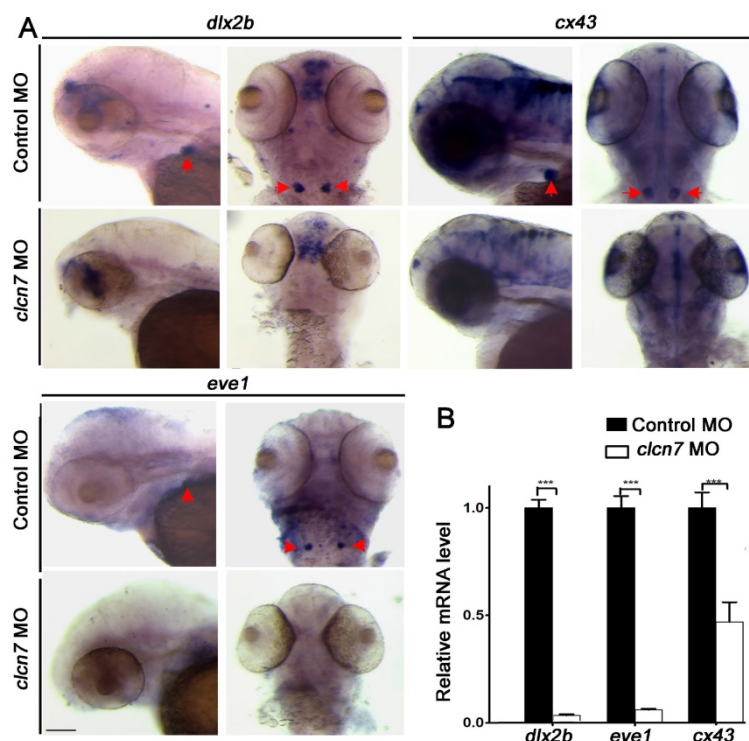


**Figure 5.** Molecular changes in the teeth of *clcn7*-deficient zebrafish. (A-B) WISH and Q-PCR analysis results. The fair expression of *dlx2b*, *cx43*, and *eve1* in the teeth of *clcn7* morphants at 3 dpf were diminished compared to that in control morphants. The data in image B was one of the representative experimental results. Error bar represents the SD. Control MO n=50, *clcn7* MO n=50. The experiment was repeated thrice with the same conditions. \*\*\*  $p < 0.001$ . Scale bars: 100  $\mu$ m.

and 7.78%, respectively (Figure 7I). Consistent with these findings, we found significant rescued tooth phenotypes in SB431542-treated *clcn7* morphants (Figure 7E-H). 98% of SB431542-treated *clcn7*

morphants had 4V<sup>1</sup> tooth compared to 70% of *clcn7* deficient embryos under DMSO treatment (Figure 7J). Thus, SB431542 treatment prevented the severity of craniofacial bone and tooth defects to some extent.

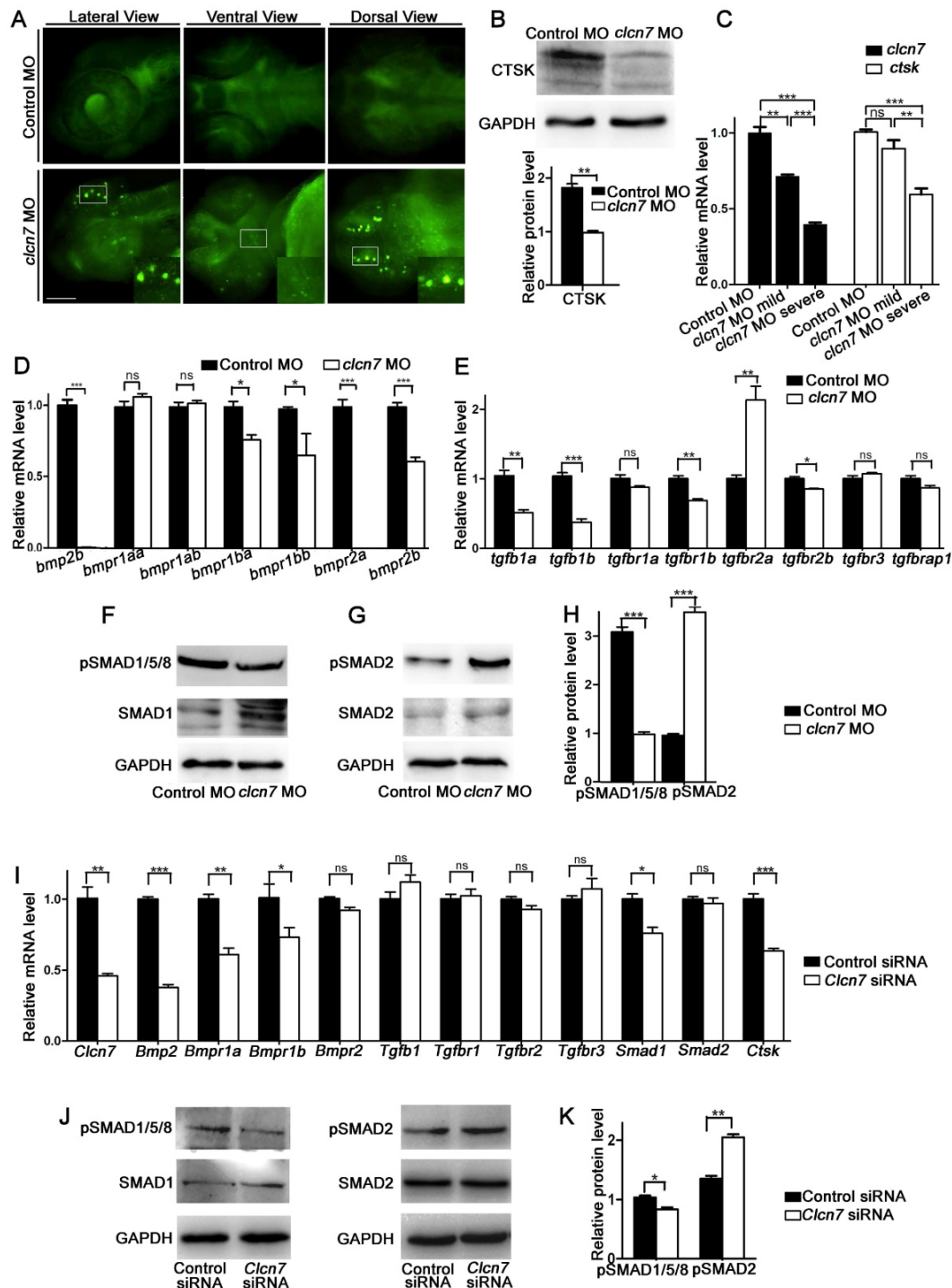


**Figure 6.** *clcn7* deficiency led to lysosomal storage, reduced Cathepsin K expression and imbalanced TGF-β/BMP signaling pathway. (A) LysoTracker staining revealed lysosomal storage in the brain and jaw in *clcn7* morphants at 3dpf compared to control morphants. The insets showed higher magnification of the white boxed areas in *clcn7* morphants. (B) Western blot and quantification analysis showed that CTSK protein was markedly decreased in *clcn7* morphants at 3dpf. (C) Comparison of *clcn7* and *ctsk* level using Q-PCR detection. The mRNA level of *clcn7* and *ctsk* showed a dose-dependent parallel downregulation with severe craniofacial changes. (D, E) Q-PCR analysis results. Transcript levels of *bmp2b* and *bmpr1aa* and *bmpr1ab*, *bmpr1ba*, *bmpr1bb*, *bmpr2a*, *bmpr2b* were decreased, the levels of *tgfb1a*, *tgfb1b* were declined and that of *tgfb2a* was increased in *clcn7* morphants compared to controls at 3dpf. (F, G and H) Western blots results. The protein levels of pSMAD 1/5/8 proteins were significantly reduced, while pSMAD2 levels were increased compared to control. (I) Q-PCR results of BMSCs. Compared to controls, the transcript levels of *Bmp2* and *Bmpr1a*, *Bmpr1b*, *Smad1* and *Ctsk* were decreased in *Clcn7* siRNA group. (J, K) Western blot analysis showed that *Clcn7* siRNA increased the protein levels of pSMAD2, while pSMAD1/5/8 levels were reduced compared to controls. For B-H: Control MO n=50, *clcn7* MO n=50, *clcn7* MO mild n=50, *clcn7* MO severe n=50. All data represent mean ±SD. The experiment was repeated at least thrice with the same conditions. ns: not significant difference. \* p<0.05, \*\* p<0.01, \*\*\* p<0.001. Scale bars: 100 μm.

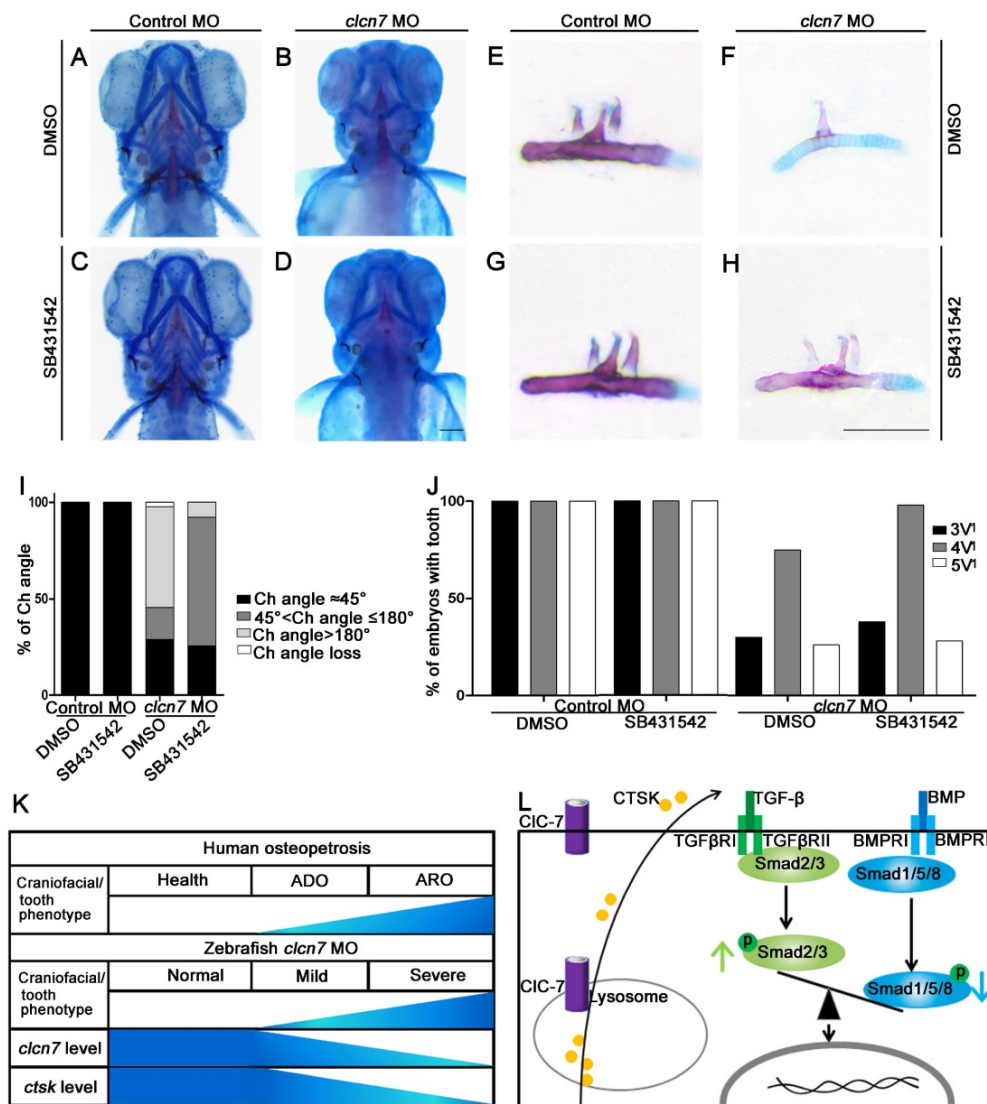


**Figure 7. Inhibition of TGF-β signaling partially rescues craniofacial abnormalities in *clcn7* deficient zebrafish.** (A-D) Ventral views of 5dpf zebrafish with alcian blue and alizarin red staining. Control zebrafish treated with DMSO (A) or 10 μM SB431542 (C) showed no obvious changes of Ch angle. (B) *clcn7* knockdown zebrafish treated with DMSO showed abnormal Ch angle, and 10 μM SB431542 partially rescued Ch angle, showing significant differences (D, I). (E-H) Comparison of embryonic tooth number among controls and *clcn7* morphants treated with DMSO or 10 μM SB431542. (J) *clcn7* morphants treated with 10 μM SB431542 showed the higher eruption rate of 4V<sup>1</sup> tooth. (K) Schematic correlation between the amount of CIC-7 and craniofacial/tooth phenotypes in humans and zebrafish. ARO showed more severe craniofacial/tooth phenotypes than ADO. The more severe the craniofacial phenotypes in *clcn7* morphants, the lower level of *clcn7* and *ctsk*, which further results in the imbalance between TGF-β and BMP signals, affecting the craniofacial and tooth development. (L) Schematic representation of CIC-7- and CTSK-mediated TGF-β/BMP pathway in zebrafish. *clcn7* deficiency led to impaired lysosomal function and reduced CTSK expression. TGF-β-like Smad2 signals are elevated and BMP-like Smad1/5/8 signals are reduced in *clcn7* knockdown zebrafish, which may contribute to the imbalance in TGF-β/BMP signaling during craniofacial and tooth development. The experiment was repeated thrice with the same conditions. The data in image J was one of the representative experimental results. For A-J: Control MO DMSO n=210, Control MO SB431542 n=198, *clcn7* MO DMSO n=158, *clcn7* MO SB431542 n=134. Scale bars: 100 μm.

## Discussion

Craniofacial and tooth characteristics have been reported in osteopetrosis since 1965 [42] and were summarized during early 1992 [43]. Review of the literatures and our own clinical data showed that ARO and severe ADO II osteopetrosis more likely cause craniofacial and tooth changes, which also occurred in osteopetrosis cases with *CLCN7* mutations. The typical craniofacial features in osteopetrosis with *CLCN7* mutations and in *Clcn7* mutant mice [11] suggested that CIC-7 might affect the formation pattern of craniofacial structures.

Our zebrafish results demonstrated that reduced *clcn7* signaling led to aberrations in craniofacial chondrogenesis and osteogenesis, including shorter Ch and Pq, defective Ch, abnormal Ch angle, and poorly mineralized bones. The above pharyngeal arch loss or reversal and neurocranial abnormalities mimicked the craniofacial changes in osteopetrosis patients and *clcn7*<sup>-/-</sup> mice [44,11], suggesting that the regulation of CIC-7 on the craniofacial development and pattern of craniofacial structures were conservative.

Type X collagen is expressed by hypertrophic chondrocytes during endochondral ossification. As a

bone-specific transcription factor [45], SP7 is required for the differentiation of mesenchymal stem cells and osteoblasts as well as bone formation [46]. Diseases associated with SP7, which include osteogenesis imperfecta and zebrafish *sp7* mutants, cause poor differentiation of teeth [47]. Both the intensity of alizarin red staining in craniofacial bones and teeth as well as the expression of *col10a1* and *sp7* were reduced in *clcn7* morphants, indicating that CIC-7 deficiency impaired the calcification of craniofacial bones and teeth. Clinical osteopetrosis reports and our pedigree analysis demonstrated that craniofacial bones, such as mandibles or maxilla, showed hypodysplasia or malformation, and were more liable to osteomyelitis; our study data on zebrafish are consistent with the above clinical manifestation of craniofacial bones.

Pycnodysostosis is another bone genetic disorder with increased radiographic bone density. As reported previously, the characteristics of head and craniofacial bones in pycnodysostosis patient, [48] including macrocephaly, frontal bossing, changes in the shape and proportions of facial skeleton, were similar to those of osteopetrosis patients summarized in this report. CTSK is the causative gene of pycnodysostosis [49]. *In situ* hybridization showed strong staining of *ctsk* in craniofacial regions, pharyngeal arch and Meckels cartilage of zebrafish [50]. CIC-7 locates lysosomes in most cell types [10,51]. *clcn7* knockdown in zebrafish showed lysosomal storage, which is consistent with previous studies in *Cln7/Ostm1* gene knockout mice [10,23,24], and the cells lacking either CIC-7 or OSTM1[23,48]. The protease activity of CTSK relies much on intracellular conditions such as lysosomal pH. Therefore, lysosomal storage of *clcn7* knockdown of zebrafish is probably the key for the impairment of the expression and activity of CTSK.

The clinical variations of osteopetrosis with *CLCN7* mutations have been previously reported [52,53] and noticed in our patients as well. Here, we also found that the variable phenotypes of craniofacial bones were related to the amount of CIC-7 and CSTK. The connection between CIC-7 and CSTK was the key influential factor for craniofacial bone development and pattern formation (**Figure 6C** and **Figure 7K**).

The impact of BMPs on zebrafish development has been explored in the past decades [54-56]. BMP signals, such as *bmp2a*, *bmp2b*, and *bmp4*, existed in zebrafish pharyngeal teeth during initiation and morphogenesis stages. BMP signaling is required for cranial development, including lower jaw, ventral arch and palate [17,57,58], and tooth formation [59,60]. In addition to BMP signaling pathway, TGF- $\beta$  signaling pathway also contributes to the development of craniofacial bone and tooth as well as several

patterning events during early embryonic development, including proper craniofacial development [61], neurocranial and pharyngeal arch chondrogenesis [62]. Imbalance between TGF- $\beta$  and BMP signaling causes secondary craniofacial malformations in mucopolipidosis II [63], which was also found in our *clcn7* morphants. BMSCs were the major cells involved in bone development, and we further confirmed that CIC-7 deficiency also resulted in the imbalance between TGF- $\beta$  and BMP signaling pathways at the cellular level of BMSCs. Together, CIC-7 deficiency impaired lysosomal condition-dependent CTSK, which may in turn modulate TGF- $\beta$ /BMP signaling to regulate early craniofacial bone development and pattern formation (**Figure 7L**).

Of the 80 osteopetrosis cases, 84% presented tooth abnormalities. Our clinical and mice data also confirmed that CIC-7 deficiency resulted in tooth abnormalities such as tooth dysplasia, impacted teeth, and root dysplasia. We further demonstrated the conservative function of CIC-7 in the regulation of tooth formation. *dlx2b* belongs to distal-less (Dlx) family and plays a role in the development of forebrain, craniofacial and tooth [64] as well as split-hand/foot formation [65]. The reduced *dlx2b* mRNA level might explain tooth malformation and tooth agenesis in *clcn7* morphants, as well as tooth problems of osteopetrosis with *CLCN7* mutations.

Another striking feature was that enameloid dysplasia and hypocalcification in *clcn7* morphants matched the high ratio of enamel dysplasia in osteopetrosis cases. *eve1* is required for the differentiation of ameloblasts and for the initiation and morphogenesis of the first tooth in zebrafish [35]. *cx43* encodes connexin 43 in zebrafish, and reduced levels of Cx43 resulted in ameloblast dysregulation, enamel hypoplasia, and secondary tissue responses [66]. The reduced mRNA levels of *eve1*, *cx43*, and mineralization-related molecule *sp7* might explain the morphological and calcification changes of enamel.

## Conclusion

In conclusion, *clcn7* acts as a key factor for the regulation of craniofacial bone and tooth formation by targeting lysosomes, CTSK and downstream TGF- $\beta$ /BMP signaling pathway. Our study provided new insights into the regulatory mechanisms of *clcn7* in zebrafish craniofacial embryonic bone and tooth development, and put forward a mechanism chain of CIC-7/CTSK/TGF- $\beta$ /BMP/SMAD to explain the typical craniofacial bone and tooth changes in osteopetrosis or even pycnodysostosis patients. Meanwhile, we found that the inhibitors of TGF- $\beta$  signaling pathway could rescue the craniofacial bone and tooth phenotypes in *clcn7*-deficient zebrafish.

These data suggest a new idea for the future treatment of craniofacial pathologies associated with osteopetrosis as well as pycnodysostosis.

## Abbreviations

ADO: autosomal dominant osteopetrosis; ADO II: autosomal dominant osteopetrosis, type II; ARO: autosomal recessive osteopetrosis; BMP: bone morphogenetic protein; BMSCs: bone marrow stromal cells; CIC-7: voltage-gated chloride channel 7; *CLCN7*: human CIC-7 gene; *Cln7*: mouse CIC-7 gene; *cln7*: zebrafish CIC-7 gene; *col10a1*:  $\alpha 1$  chain of collagen type X; *cx43*: connexin 43; *dlx2b*: distal-less homeobox 2b; *eve1*: even-skipped-like1; IRO: intermediate autosomal osteopetrosis; pSMAD1/5/8: phosphorylated SMAD1/5/8; pSMAD2: phosphorylated SMAD2; Q-PCR: quantitative real time polymerase chain reaction; *sp7*: Sp7 transcription factor; TGF- $\beta$ : transforming growth factor  $\beta$ ; WISH: whole-mount *in situ* hybridization.

## Acknowledgements

This work was supported by the National Natural Science Foundation of China (NSFC Nos. 81771052, 81271116, 81470728, 31601838). We thank for the agreement of the patients and the controls to join in this research.

## Supplementary Material

Supplementary tables.

<http://www.thno.org/v09p1387s1.pdf>

## Competing Interests

The authors have declared that no competing interest exists.

## References

1. Stark Z, Savarirayan R. Osteopetrosis. *Orphanet J Rare Dis*. 2009;4:5.
2. Campos-Xavier AB, Saraiva JM, Ribeiro LM, Munnich A, Cormier-Daire V. Chloride channel 7 (*CLCN7*) gene mutations in intermediate autosomal recessive osteopetrosis. *Hum Genet*. 2003;112:186-89.
3. Zhang XY, He JW, Fu WZ, Wang C, Zhang ZL. Novel mutations of *TCIRG1* cause a malignant and mild phenotype of autosomal recessive osteopetrosis (ARO) in four Chinese families. *Acta Pharmacol Sin*. 2017;38:1456-65.
4. Del FA, Cappariello A, Teti A. Genetics, pathogenesis and complications of osteopetrosis. *Bone*. 2008;42:19-29.
5. Frattini A, Pangrazio A, Susani L, Sobacchi C, Mirolo M, Abinun M, et al. Chloride channel *CLCN7* mutations are responsible for severe recessive, dominant, and intermediate osteopetrosis. *J Bone Miner Res*. 2003;18:1740-47.
6. Xue Y, Wang W, Mao T, Duan X. Report of two Chinese patients suffering from *CLCN7*-related osteopetrosis and root dysplasia. *J Craniomaxillofac Surg*. 2012;40:416-20.
7. Wang H, Pan M, Ni J, Zhang Y, Zhang Y, Gao S, et al. *CIC-7* Deficiency impairs tooth development and eruption. *Sci Rep*. 2016;6:19971.
8. Duan X. Ion channels, channelopathies, and tooth formation. *J Dent Res*. 2014;93:117-25.
9. Lu X, Rios HF, Jiang B, Xing L, Kadlcek R, Greenfield EM, et al. A new osteopetrosis mutant mouse strain (*ntl*) with odontoma-like proliferations and lack of tooth roots. *Eur J Oral Sci*. 2009;117:625-35.
10. Kornak U, Kasper D, Bosl MR, Kaiser E, Schweizer M, Schulz A, et al. Loss of the *CIC-7* chloride channel leads to osteopetrosis in mice and man. *Cell*. 2001;104:205-15.
11. Wen X, Lacruz RS, Paine ML. Dental and cranial pathologies in mice lacking the *Cl(-)/H(+)*-exchanger *CIC-7*. *Anat Rec (Hoboken)*. 2015;298:1502-08.
12. Detailleur V, Vansteenkiste G, Renard M, Verdonck A. Dental care approach in patients with osteopetrosis. *Eur Arch Paediatr Dent*. 2016;17:435-43.
13. Walshe J, Mason I. Fgf signalling is required for formation of cartilage in the head. *Dev Biol*. 2003;264:522-36.
14. Wada N, Javidan Y, Nelson S, Carney TJ, Kelsh RN, Schilling TF. Hedgehog signaling is required for cranial neural crest morphogenesis and chondrogenesis at the midline in the zebrafish skull. *Development*. 2005;132:3977-88.
15. Brault V, Moore R, Kutsch S, Ishibashi M, Rowitch DH, McMahon AP, et al. Inactivation of the beta-catenin gene by *Wnt1-Cre*-mediated deletion results in dramatic brain malformation and failure of craniofacial development. *Development*. 2001;128:1253-64.
16. Jayasena CS, Bronner ME. *Rbms3* functions in craniofacial development by posttranscriptionally modulating TGF-beta signaling. *J Cell Biol*. 2012;199:453-66.
17. Alexander C, Zuniga E, Blitz IL, Wada N, Le Pabic P, Javidan Y, et al. Combinatorial roles for BMPs and Endothelin 1 in patterning the dorsal-ventral axis of the craniofacial skeleton. *Development*. 2011;138:5135-46.
18. Saftig P, Hunziker E, Wehmeyer O, Jones S, Boyde A, Rommerskirch W, et al. Impaired osteoclastic bone resorption leads to osteopetrosis in cathepsin-K-deficient mice. *Proc Natl Acad Sci U S A*. 1998;95:13453-58.
19. Chen MF, Chen TY. Different fast-gate regulation by external *Cl(-)* and *H(+)* of the muscle-type *CIC* chloride channels. *J Gen Physiol*. 2001;118:23-32.
20. Neutzsky-Wulff AV, Karsdal MA, Henriksen K. Characterization of the bone phenotype in *CIC-7*-deficient mice. *Calcif Tissue Int*. 2008;83:425-37.
21. Sartelet A, Stauber T, Coppieters W, Ludwig CF, Fasquelle C, Druet T, et al. A missense mutation accelerating the gating of the lysosomal *Cl(-)/H(+)*-exchanger *CIC-7/Ostm1* causes osteopetrosis with gingival hamartomas in cattle. *Dis Model Mech*. 2014;7:119-28.
22. Weinert S, Jabs S, Hohensee S, Chan WL, Kornak U, Jentsch TJ. Transport activity and presence of *CIC-7/Ostm1* complex account for different cellular functions. *EMBO Rep*. 2014;15:784-91.
23. Kasper D, Planells-Cases R, Fuhrmann JC, Scheel O, Zeitz O, Ruether K, et al. Loss of the chloride channel *CIC-7* leads to lysosomal storage disease and neurodegeneration. *EMBO J*. 2005;24:1079-91.
24. Lange PF, Wartosch L, Jentsch TJ, Fuhrmann JC. *CIC-7* requires *Ostm1* as a beta-subunit to support bone resorption and lysosomal function. *Nature*. 2006;440:220-23.
25. Zhang Y, Ke Y, Zheng X, Liu Q, Duan X. Correlation between genotype and phenotype in three families with Peutz-Jeghers Syndrome. *Exp Ther Med*. 2017;13:507-14.
26. Cleiren E, Benichou O, Van Hul E, Gram J, Bollerslev J, Singer FR, et al. Albers-Schonberg disease (autosomal dominant osteopetrosis, type II) results from mutations in the *CICN7* chloride channel gene. *Hum Mol Genet*. 2001;10:2861-67.
27. Zhang Y, Zhang Y, Zheng X, Xu R, He H, Duan X. Grading and quantification of dental fluorosis in zebrafish larva. *Arch Oral Biol*. 2016;70:16-23.
28. Santos-Ledo A, Garcia-Macia M, Campbell PD, Gronska M, Marlow FL. Kinesin-1 promotes chondrocyte maintenance during skeletal morphogenesis. *PLoS Genet*. 2017;13:e1006918.
29. Zhao W, Zhang Y, Yang S, Hao Y, Wang Z, Duan X. Analysis of two transcript isoforms of vacuolar ATPase subunit H in mouse and zebrafish. *Gene*. 2018;638:66-75.
30. Duan X, Liu J, Zheng X, Wang Z, Zhang Y, Hao Y, et al. Deficiency of *ATP6V1H* causes bone loss by inhibiting bone resorption and bone formation through the TGF- $\beta$ 1 pathway. *Theranostics*. 2016;6:2183-95.
31. Thisse C, Thisse B. High-resolution *in situ* hybridization to whole-mount zebrafish embryos. *Nat Protoc*. 2008;3:59-69.
32. Li L, Yang S, Zhang Y, Ji D, Jin Z, Duan X. *ATP6V1H* regulates the growth and differentiation of bone marrow stromal cells. *Biochem Biophys Res Commun*. 2018;502:84-90.
33. Waguespack SG, Hui SL, Dimeglio LA, Econs MJ. Autosomal dominant osteopetrosis: clinical severity and natural history of 94 subjects with a chloride channel 7 gene mutation. *J Clin Endocrinol Metab*. 2007;92:771-78.
34. Jackman WR, Draper BW, Stock DW. Fgf signaling is required for zebrafish tooth development. *Dev Biol*. 2004;274:139-57.
35. Laurenti P, Thaeon C, Allizard F, Huyseune A, Sire JY. Cellular expression of *evr1* suggests its requirement for the differentiation of the ameloblasts and for the initiation and morphogenesis of the first tooth in the zebrafish (*Danio rerio*). *Dev Dyn*. 2004;230:727-33.
36. DeLaurier A, Eames BF, Blanco-Sanchez B, Peng G, He X, Swartz ME, et al. Zebrafish *sp7:EGFP*: a transgenic for studying otic vesicle formation, skeletogenesis, and bone regeneration. *Genesis*. 2010;48:505-11.
37. Chen X, Zhang K, Hock J, Wang C, Yu X. Enhanced but hypofunctional osteoclastogenesis in an autosomal dominant osteopetrosis type II case carrying a c.1856C>T mutation in *CLCN7*. *Bone Res*. 2016;4:16035.
38. Goldring MB, Tsuchimochi K, Ijiri K. The control of chondrogenesis. *J Cell Biochem*. 2006;97:33-44.
39. Inman GJ, Nicolás FJ, Callahan JF, Harling JD, Gaster LM, Reith AD, et al. SB-431542 is a potent and specific inhibitor of transforming growth factor- $\beta$  superfamily type I activin receptor-like kinase (ALK) receptors ALK4, ALK5, and ALK7. *Mol Pharmacol*. 2002;62:65-74.
40. Chablais F, Jazwinska A. The regenerative capacity of the zebrafish heart is dependent on TGFbeta signaling. *Development*. 2012;139:1921-30.

41. Ho DM, Chan J, Bayliss P, Whitman M. Inhibitor-resistant type I receptors reveal specific requirements for TGF-beta signaling in vivo. *Dev Biol.* 2006;295:730-42.
42. Francisco JV, Reichman L. Osteopetrosis with a complication osteomyelitis of the mandible. Report of a case. *Oral Surg Oral Med Oral Pathol.* 1965;19:462-5.
43. Elster AD, Theros EG, Key LL, Chen MY. Cranial imaging in autosomal recessive osteopetrosis. Part II. Skull base and brain. *Radiology.* 1992;183:137-44.
44. Kornak U, Kasper D, Bosl MR, Kaiser E, Schweizer M, Schulz A, et al. Loss of the ClC-7 chloride channel leads to osteopetrosis in mice and man. *Cell.* 2001;104:205-15.
45. DeLaurier A, Eames BF, Blanco-Sanchez B, Peng G, He X, Swartz ME, et al. Zebrafish sp7:EGFP: a transgenic for studying otic vesicle formation, skeletogenesis, and bone regeneration. *Genesis.* 2010;48:505-11.
46. Kimmel CB, DeLaurier A, Ullmann B, Dowd J, McFadden M. Modes of developmental outgrowth and shaping of a craniofacial bone in zebrafish. *PLoS One.* 2010;5:e9475.
47. Kague E, Witten PE, Soenens M, Campos CL, Lubiana T, Fisher S, et al. Zebrafish sp7 mutants show tooth cycling independent of attachment, eruption and poor differentiation of teeth. *Dev Biol.* 2018;435:176-84.
48. Xue Y, Wang L, Xia D, Li Q, Gao S, Dong M, et al. Dental abnormalities caused by novel compound heterozygous CTSK mutations. *J Dent Res.* 2015;94:674-81.
49. Paznekas WA, Boyadjiev SA, Shapiro RE, Daniels O, Wollnik B, Keegan CE, et al. Connexin 43 (GJA1) mutations cause the pleiotropic phenotype of oculodentodigital dysplasia. *Am J Hum Genet.* 2003;72:408-18.
50. Steinberg BE, Huynh KK, Brodovitch A, Jabs S, Stauber T, Jentsch TJ, et al. A cation counterflux supports lysosomal acidification. *J Cell Biol.* 2010;189:1171-86.
51. Weinert S, Jabs S, Supanchart C, Schweizer M, Gimber N, Richter M, et al. Lysosomal pathology and osteopetrosis upon loss of H<sup>+</sup>-driven lysosomal Cl-accumulation. *Science.* 2010;328:1401-03.
52. Pang Q, Chi Y, Zhao Z, Xing X, Li M, Wang O, et al. Novel mutations of CLCN7 cause autosomal dominant osteopetrosis type II (ADO-II) and intermediate autosomal recessive osteopetrosis (IARO) in Chinese patients. *Osteoporos Int.* 2016;27:1047-55.
53. Frattini A, Pangrazio A, Susani L, Sobacchi C, Mirolò M, Abinun M, et al. Chloride channel CLCN7 mutations are responsible for severe recessive, dominant, and intermediate osteopetrosis. *J Bone Miner Res.* 2003;18:1740-47.
54. Nie X, Luukko K, Kettunen P. BMP signalling in craniofacial development. *Int J Dev Biol.* 2006;50:511-21.
55. Zhang YD, Chen Z, Song YQ, Liu C, Chen YP. Making a tooth: growth factors, transcription factors, and stem cells. *Cell Res.* 2005;15:301-16.
56. Chen G, Deng C, Li YP. TGF- $\beta$  and BMP signaling in osteoblast differentiation and bone formation. *Int J Biol Sci.* 2012;8:272-88.
57. Zuniga E, Rippen M, Alexander C, Schilling TF, Crump JG. Gremlin 2 regulates distinct roles of BMP and Endothelin 1 signaling in dorsoventral patterning of the facial skeleton. *Development.* 2011;138:5147-56.
58. Schoenebeck JJ, Hutchinson SA, Byers A, Beale HC, Carrington B, Faden DL, et al. Variation of BMP3 contributes to dog breed skull diversity. *PLoS Genet.* 2012;8:e1002849.
59. Wise SB, Stock DW. Conservation and divergence of Bmp2a, Bmp2b, and Bmp4 expression patterns within and between dentitions of teleost fishes. *Evol Dev.* 2006;8:511-23.
60. Payne TL, Skobe Z, Yelick PC. Regulation of tooth development by the novel type I TGFbeta family member receptor Alk8. *J Dent Res.* 2001;80:1968-73.
61. Chai Y, Ito Y, Han J. TGF-beta signaling and its functional significance in regulating the fate of cranial neural crest cells. *Crit Rev Oral Biol Med.* 2003;14:78-88.
62. Cheah FS, Winkler C, Jabs EW, Chong SS. Tgfbeta3 regulation of chondrogenesis and osteogenesis in zebrafish is mediated through formation and survival of a subpopulation of the cranial neural crest. *Mech Dev.* 2010;127:329-44.
63. Flanagan-Steet H, Aarnio M, Kwan B, Guihard P, Petrey A, Haskins M, et al. Cathepsin-mediated alterations in TGF $\beta$ -related signaling underlie disrupted cartilage and bone maturation associated with impaired lysosomal targeting. *J Bone Miner Res.* 2016;31:535-48.
64. Dai J, Si J, Ouyang N, Zhang J, Wu D, Wang X, et al. Dental and periodontal phenotypes of Dlx2 overexpression in mice. *Mol Med Rep.* 2017;15:2443-50.
65. Theisen A, Rosenfeld JA, Shane K, McBride KL, Atkin JF, Gaba C, et al. Refinement of the region for split hand/foot malformation 5 on 2q31.1. *Mol Syndromol.* 2010;1:262-71.
66. Toth K, Shao Q, Lorentz R, Laird DW. Decreased levels of Cx43 gap junctions result in ameloblast dysregulation and enamel hypoplasia in Cx43<sup>fl/fl</sup> mice. *J Cell Physiol.* 2010;223:601-9.